Bridge damage identification under varying environmental and operational conditions combining Deep Learning and numerical simulations

Ana Fernandez-Navamuel[a,b,c], David Pardo[c,b,d], Filipe Magalhães[e], Diego Zamora-Sánchez[a], Ángel J. Omella[c], David Garcia-Sanchez[a]

[a]*TECNALIA, Basque Research and Technology Alliance (BRTA), Parque Científico y Tecnológico de Bizkaia, Astondo bidea, Edificio 700, E- 48160 Derio, Spain*
[b]*Basque Center for Applied Mathematics (BCAM), Bilbao, Spain*
[c]*University of the Basque Country (UPV/EHU) Leioa, Spain*
[d]*Ikerbasque (Basque Foundation for Sciences), Bilbao, Spain*
[e]*CONSTRUCT-ViBest, Faculty of Engineering, University of Porto (FEUP), Rua Dr. Roberto Frias 4200-465 Porto, Portugal*

Abstract

This work proposes a novel supervised learning approach to identify damage in operating bridge structures. We propose a method to introduce the effect of environmental and operational conditions into the synthetic damage scenarios employed for training a Deep Neural Network, which is applicable to large-scale complex structures. We apply a clustering technique based on Gaussian Mixtures to effectively select Q representative measurements from a long-term monitoring dataset. We employ these measurements as the target response to solve various Finite Element Model Updating problems before generating different damage scenarios. The synthetic and experimental measurements feed two Deep Neural Networks that assess the structural health condition in terms of damage severity and location. We demonstrate the applicability of the proposed method with a real full-scale case study: the Infante Dom Henrique bridge in Porto. A comparative study reveals that neglecting different environmental and operational conditions during training detracts the damage identification task. By contrast, our method provides successful results during a synthetic validation.

Keywords: Structural Health Monitoring, Damage Identification, Deep Learning, Varying Environmental and Operational Conditions

1. Introduction

Structural Health Monitoring (SHM) is the process of continuously assessing the health condition of a structure (e.g., a bridge B) based on monitoring data to detect and identify the presence of damage [1]. In SHM, identifying damage is an inverse problem where we seek to infer the true bridge condition D_B from the response measurements ($\mathbf{m}_B$)

obtained through monitoring, such that:

$$D_B = \mathcal{I}(\mathbf{m}_B), \qquad (1)$$

where $\mathcal{I}$ denotes the inverse operator. According to [2], there exist four levels in damage identification: detection, location, quantification, and forecasting.

In large civil engineering structures, such as bridges, raw monitoring data may come from sensors of different natures and contain numerous uncertainty sources [3]. Deciding what to measure is critical when implementing SHM for damage identification. The measured observations $\mathbf{m}_B = \mathbf{u}_B + \boldsymbol{\epsilon}$ contain the structural response $\mathbf{u}_B$ and measurement error $\boldsymbol{\epsilon}$. They must be sensitive to damage for the SHM strategy to be effective. In operating bridges, many phenomena exist that make $\mathbf{u}_B$ fluctuate over time, regardless of the health condition. These are Environmental and Operational Conditions (EOCs) and include temperature, humidity, or traffic level [4, 5, 6]. The structural response contains two affecting terms, i.e., $\mathbf{u}_B = f(\mathbf{u}_{Dam}, \mathbf{u}_{EOC})$, where $\mathbf{u}_{Dam}$ accounts for the effect of damage and $\mathbf{u}_{EOC}$ refers to the effect of varying EOCs. An ideal measurement would be sensitive to damage but poorly affected by EOCs. However, this is not often the case, and both phenomena coexist [6]. The effect of EOCs may mask the presence of damage or raise false alerts, hindering the assessment task [7, 8, 9, 10]. Thus, handling EOCs has become one of the main challenges in transitioning SHM practices from the laboratory domain to the full-scale application [11].

There are two broad approaches to damage identification: model-based and data-driven [12]. Model-based approaches rely on numerical approximations, mainly Finite Element (FE) models, to assess the structural condition. They employ an iterative procedure such as Finite Element Model Updating (FEMU) [13]. By changing some structural properties, FEMU minimizes the discrepancy between the analytical response and that measured in the target structure [13, 14].

Many works employing model-based assessment neglect the effect of varying EOCs and focus on deterministic FEMU techniques [15, 16, 17, 18, 19, 20]. In [21], Moaveni and Behmanesh study the effect of changing EOCs in standard FEMU and demonstrate that uncertainty propagates during the updating, yielding wrong predictions. A powerful approach to tackle varying EOCs in the model-based domain is bayesian FEMU [22, 23, 24, 25, 26, 27, 28, 29, 30]. However, the main limitation of damage identification approaches based on FEMU is its high computational cost. Solving the inverse problem requires intensive computational calculations and prevents a real-time assessment [31]. Some works, such as [32, 33], employ surrogated models to hasten the updating process.

As an alternative, data-driven methods employ measurements from monitoring systems and provide assessment regardless of the physics governing

2

the structural behavior [1]. They are suitable when long-term monitoring data are available to establish a baseline on the reference structural condition [34]. They present the advantage of producing close to real-time assessment since they avoid FE simulations. Data-driven approaches have evolved over the years, from statistical pattern recognition methods [34, 35] to robust Artificial Intelligence-based methods [36]. The irruption of Deep Learning (DL) methods has settled a new paradigm in the field of SHM, given their capability to accurately approximate complex problems [37, 38]. DL methods require offline training to learn the desired relationship and find the model parameters [37]. In data-driven methods, handling the effect of varying EOCs is also challenging [39, 40, 41]. The goal is to separate the contribution of EOCs ($\mathbf{u}_{EOC}$) from that of damage ($\mathbf{u}_{Dam}$) on the measured structural response. Methods such as Principal Component Analysis (PCA) have been widely applied in this task [42, 43, 44, 45, 46]. Some recent works, such as [47] or [48], employ more sophisticated approaches based on DL to enhance the performance of PCA.

The main limitation of data-based methods is the impossibility of accessing data from different damage scenarios. This data scarcity enforces them to remain in the unsupervised category [49]. In the context of SHM, unsupervised means that only level I is attainable according to Rytter scale [2]. Several works have been published on unsupervised SHM applications using data-driven methods

[50, 49, 51, 52].

In light of this situation, hybrid approaches have been explored [53, 54, 55, 56, 57, 58, 59]. Hybrid approaches combine monitoring data with computational simulations and employ both data-driven and model-based techniques [57]. These methods incorporate unmeasurable scenarios through FE simulations to enrich the training phase of data-driven methods [60]. The goal is to provide high-level identification (level III [2]) while preserving the advantage of yielding close to real-time assessment. However, most works addressing hybrid assessment strategies apply to laboratory-scale structures, and their practicability in operating bridges still needs to be explored.

In our previous work [59], we proposed a hybrid approach for damage identification in bridges. We drove the methodology towards its applicability in large structural systems under service but neglected the effect of changing EOCs in the synthetic damage scenarios used for training a Deep Neural Network for real-time assessment. Here, we enhance our previous work [59] by incorporating the effect of varying EOCs in the synthetic damage scenarios using long-term monitoring data. We apply a clustering algorithm based on a Gaussian Mixture Model (GMM) to classify healthy data into Q groups that represent different EOCs. We identify one representative measurement for each cluster and apply FEMU to obtain the Q corresponding updated parametrizations. The FEMU proce-

3

dures reduce model uncertainty and approximate the measured responses to represent each particular EOC. We follow the procedure developed in [59] for each updated parametrization to obtain synthetic scenarios labeled by damage severity and location. The synthetic database now incorporates damage scenarios occurring under different EOCs, which is the main contribution of this work. We finally employ two separate DNNs as the data-driven assessment method. We first estimate the damage severity. If the estimated severity exceeds a predefined threshold value indicating damage, we estimate its location.

We found two hybrid approaches in the literature tackling the effect of varying EOCs [61, 57]. Liu and Zhang [61] also employ GMM to classify experimental eigenfrequencies in a cable-stayed bridge. However, they apply a model-based assessment strategy that prevents a fast diagnostic. Instead, our hybrid methodology provides close to real-time assessment once the DNNs undergo adequate training. On the other hand, Figueiredo et al. [57] propose a hybrid methodology that combines FE simulations and Machine Learning (ML) to assess the health condition of a bridge. Their work remains in the unsupervised learning domain since they include no damage scenarios.

Our work provides a new methodology that is applicable for full-scale complex structures in the task of damage identification under varying EOCs. Using computational parametrizations to recreate the damage scenarios poses one limitation to this work since it introduces modeling errors and uncertainties that affect the assessment. However, we expect these errors to be sufficiently small compared to the effect of damage. In addition, a restrictive trade-off exists between the number of employed measurements to cover most EOC variability and the computational cost of generating the database.

We validate the methodology with data from bridge Infante Dom Henrique, a very singular arch bridge in Porto city. Given the lack of real damage scenarios, we perform synthetic testing to explore and demonstrate the capability of the proposed methodology. We compare the results obtained with the proposed methodology with those of the original approach described in [59]. Results reveal that whereas both approaches provide adequate performance in identifying damage that occurs under the EOCs considered during training, the original methodology fails for different EOCs. On the other side, the proposed methodology gains robustness in damage identification under varying EOCs.

2. Methodology

In our previous work [59], we addressed the damage identification problem as a deterministic task. We employed the response $\mathbf{m}_B^h$ acquired during a short-term ambient vibration test as the reference to update a FE parametrization. This measurement corresponds to a particular date and time

4

with specific EOCs. We then generated a synthetic database from the updated parametrization. These scenarios were assumed to occur under the same EOCs.

Figure 1 schematically represents the synthetic database for one zone in the bridge, where we generated n_s synthetic scenarios with varying damage severity within the interval $[0, 0.5]$. The same holds for the other zones. In the figure, the horizontal axis represents a dummy variable including all the involved environmental and operational factors, such as temperature, humidity, traffic, etc. This approach disregards the effect of varying EOCs in the synthetic damage scenarios database. In this paper, we aim to enhance the methodology by incorporating the effect of varying EOCs in the training database of DNNs for damage assessment.

2.1. Gaussian Mixture Model clustering

Given an instrumented structure where long-term monitoring data are available (one year or more), we have access to a set of measurements M_B that corresponds to its healthy or reference behavior. These measurements include many healthy states with different EOCs, such that $M_B = \{\mathbf{m}_B^i\}_{i=1}^{N_m}$, where N_m is the total number of healthy samples measured during the monitoring period. Each measurement contains the eigenfrequencies and eigenmodes of the structure, $\mathbf{m}_B^i = \{\mathbf{f}_B^i, \mathbf{\Phi}_B^i\}$.

Environmental and operational conditions mainly include temperature, humidity, and traffic [62]. During long-term periods, these phenomena progressively change over time with certain seasonality. Ideally, we would like to generate a synthetic database that contains scenarios occurring at any possible combination of EOCs (see Figure 2). However, achieving this database is unfeasible. It requires solving a Finite Element model updating problem for each of the N_m available measurements to obtain the corresponding calibrated parametrizations.

Alternatively, here we obtain some representative measurements that describe the entire dataset and include most EOC variation. By applying a clustering technique, we classify the long-term monitoring data into Q groups that characterize the existing variability. We employ a Gaussian Mixture Model (GMM) to address this issue [63]. A GMM is an unsupervised clustering method that classifies a dataset X according to probability density estimations on a mixture of gaussians [63]. We define the GMM as a linear combination of multivariate gaussian distributions such that the probability density function $P(X)$ is computed by:

$$P(X) = \sum_{q=1}^{Q} \pi_q \mathcal{N}(X|\mu_q, \Sigma_q), \qquad (2\text{a})$$

$$0 \leq \pi_q \leq 1, \quad \sum_{q=1}^{Q} \pi_q = 1, \qquad (2\text{b})$$

where $\mathcal{N}$ stands for the gaussian distribution, and π_q indicates the mixing coefficient or weight for the q-th gaussian represented by its mean μ_q and covariance matrix Σ_q [63].
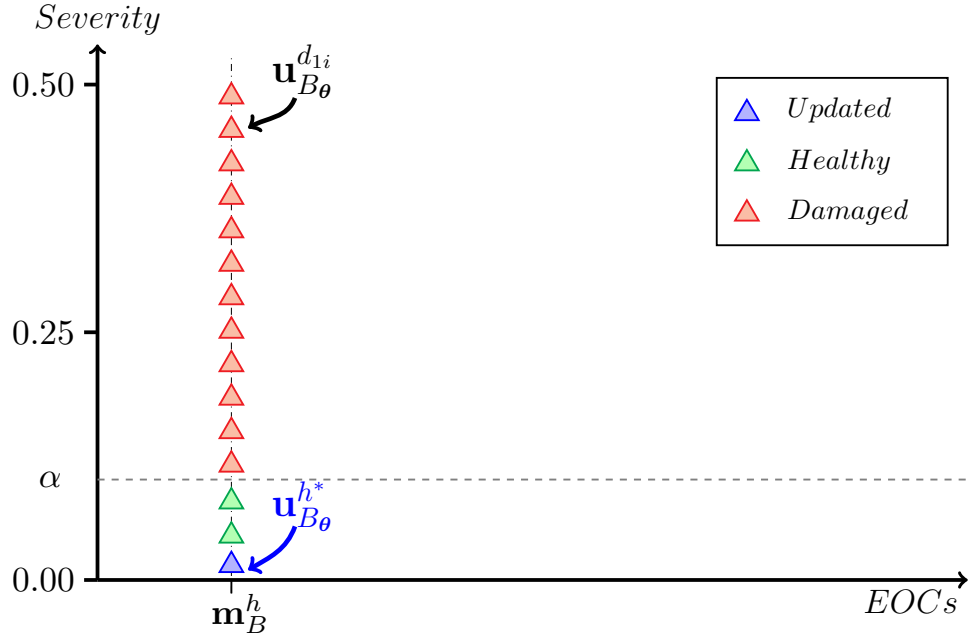
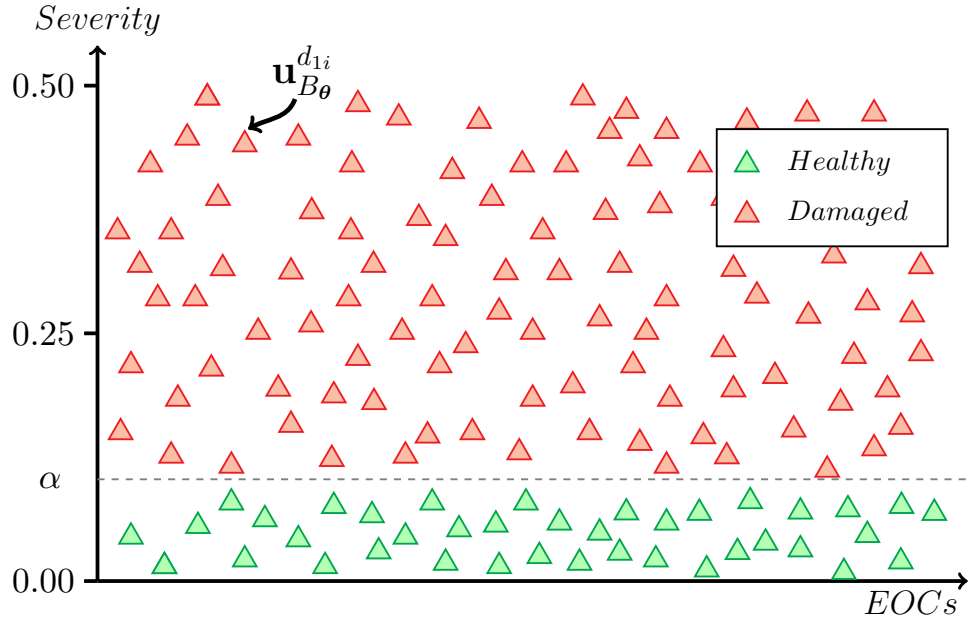Figure 1: Original synthetic database representation

Figure 2: Ideal synthetic database representation

The GMM determines the linear combination of gaussian functions that best separates the measurements into Q clusters using the Expectation Maximization algorithm [63, 64]. Each of these groups is expected to represent a set of EOCs sharing some common characteristics (e.g., high temperatures).

The number of clusters is often decided based on metrics such as the Maximum log-likelihood [64]. Figure 3 shows an example of a GMM classification for two-dimensional measurements in X with $Q = 3$ clusters. Here, we apply a Q-dimensional GMM to the available monitoring data M_B. Each measurement belongs to a cluster based on the highest probability among the Q gaussians. We obtain a representative point for each cluster as that with minimal distance to the corresponding gaussian mean:

$$\mathbf{m}_B^{h_q} := \underset{\mathbf{m}_B}{\arg\min}(\rho_{\mathbf{m}_B}^q), \qquad q = 1, 2, ..., Q \quad (3)$$

where we calculate the distance as $\rho_{\mathbf{m}}^q = \sqrt{\sum_{j=1}^{v}(m_{B_j} - \mu_j^q)^2}$, with v indicating the dimension of the vectors. We select these representative measurements: $\{\mathbf{m}_B^{h_1}, \mathbf{m}_B^{h_2}, ..., \mathbf{m}_B^{h_Q}\}$. This approach sets a trade-off between the number of clusters and the computational cost of building the database. Figure 4 schematically represents the proposed database for one zone in the bridge. The same holds for the other zones. The selected measurements are representative according to the GMM clustering. We thus expect that they cover most EOC variability.

For each of the Q selected representative measurements, we apply the same procedure developed in our previous work [59] to obtain the synthetic datasets under different EOCs. Sections 2.2 to 2.5 summarize the methodology step by step. A more detailed description can be found in [59].

2.2. Bridge parametrization

We build a computational representation of the bridge using a FE parametrization. We denote by $B_{\boldsymbol{\theta}} = \{\boldsymbol{\theta}_1, ..., \boldsymbol{\theta}_{n_z}\}$ to a parametrization of the bridge B with n_z different zones. The parametrization describes the behavior of the structure and includes elastic material properties, cross-sections, and spring constants modeling the boundary conditions. We describe each zone B_{θ} by a subset of properties, namely: $\boldsymbol{\theta}_i = \{\theta_1, ..., \theta_{n_{\theta_i}}\}$. We apply a FE solver $\mathcal{F}^{FE}$ to solve the eigenproblem and obtain the dynamic response of the parametrization $B_{\boldsymbol{\theta}}$:

$$\mathbf{u}_{B_{\theta}} = \mathcal{F}^{FE}(B_{\theta}), \qquad (4)$$

where $\mathbf{u}_{B_{\theta}} = \{\mathbf{f}_{B_{\theta}}, \phi_{B_{\theta}}\}$ contains the parametrization eigenfrequencies and eigenmodes. For the sake of simplicity, we denote $\mathcal{F}^{FE}$ by $\mathcal{F}$.

2.3. Updating procedure for Q healthy states

Under normal operating conditions, we assume the bridge is healthy and has a dynamic response $\mathbf{u}_{B^h} = \{\mathbf{f}_{B_u}, \phi_{B_u}\}$. In large-scale structures, we often measure $\mathbf{u}_B^h$ through a short-term ambient vibration test with some inherent error: $\mathbf{m}_B^h = \mathbf{u}_B^h + \epsilon$. We subsequently obtain the dynamic properties using Operational Modal Analysis (OMA) techniques, yielding $\mathbf{m}_B'^h = \{\mathbf{f}_B^h, \phi_B^h\}$ [65, 66]. For simplicity in notation, we remove the tilde and refer to the OMA-processed response as $\mathbf{m}_B^h$.

We initialize the parametrization properties to $B_{\theta} = B_{\theta_0}$, based on engineering knowledge and de-
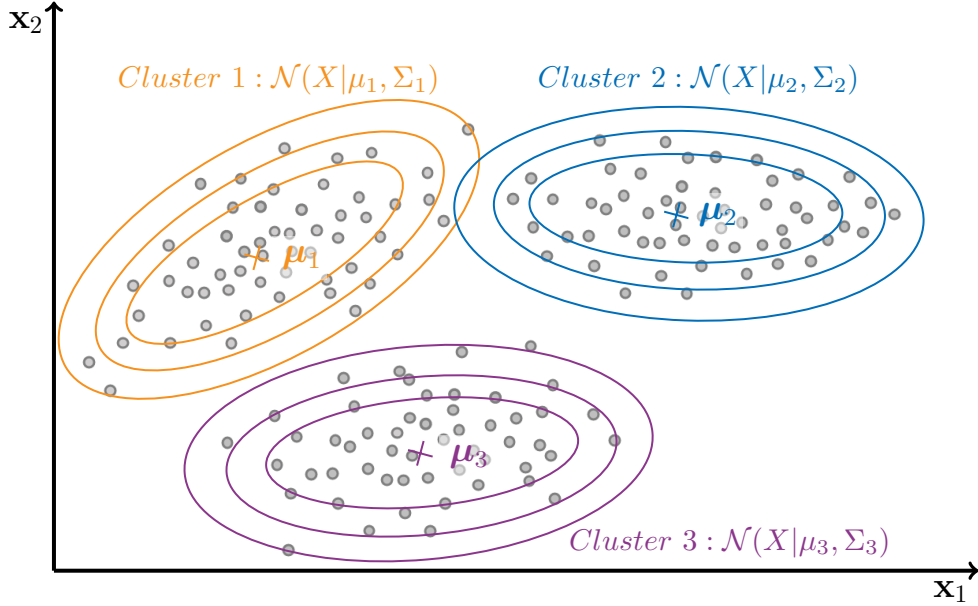
Figure 3: Example of GMM clustering with two-dimensional data

sign specifications. We obtain the corresponding structural response as $\mathbf{u}_{\theta_0} = \mathcal{F}(B_{\theta_0})$. However, $\mathbf{u}_{\theta_0}$ is in general far from $\mathbf{u}_B^h$, mainly due to uncertainties in the true material properties of B and assumptions in the boundary conditions. The updating process yields a parametrization B_θ^* whose response $\mathbf{u}_{B_\theta^*}$ approximates $\mathbf{u}_B^h$ with reduced error. We address this inverse problem by minimizing the discrepancy between both responses (computational and experimental) using the l_2 norm:

$$B_\theta^* := \arg\min_{B_\theta} \|\mathcal{F}(B_\theta) - \mathbf{u}_B^h\|_2. \qquad (5)$$

We establish the variation intervals for B_θ to ensure a physically meaningful solution representing the healthy state. We repeat the updating step Q times to obtain the corresponding calibrated parametrizations that match each representative measurement.

2.4. Damage simulation

We divide the bridge B into n_z zones where we aim to locate damage. We assume that only one zone experiments damage at a given time. For a damage occuring at the i-th zone, the location is given by $L_{B_\theta} = i$. We define a reduction vector $\boldsymbol{\alpha}_i \in [\mathbf{l}_i, 1]^{n_{\theta_i}}$ that affects the structural properties as:

$$\boldsymbol{\theta}_i^d = \boldsymbol{\alpha}_i \boldsymbol{\theta}_i^*, \qquad (6)$$

where the lower bounds $\mathbf{l}_i \in \mathbb{R}^{n_{\theta_i}}$ contain the maximum reduction value of the properties in $\boldsymbol{\theta}_i$ to ensure structural meaning. We maintain the remaining subsets of properties $\boldsymbol{\theta}_j$ $(j \neq i)$ to their undamaged value in B_θ^*. Hence, for a certain damage scenario, we obtain the parametrization at the i-th zone as $B_\theta^d = \{\boldsymbol{\theta}_1^*, ..., \boldsymbol{\theta}_i^d, ..., \boldsymbol{\theta}_{n_z}^*\}$.
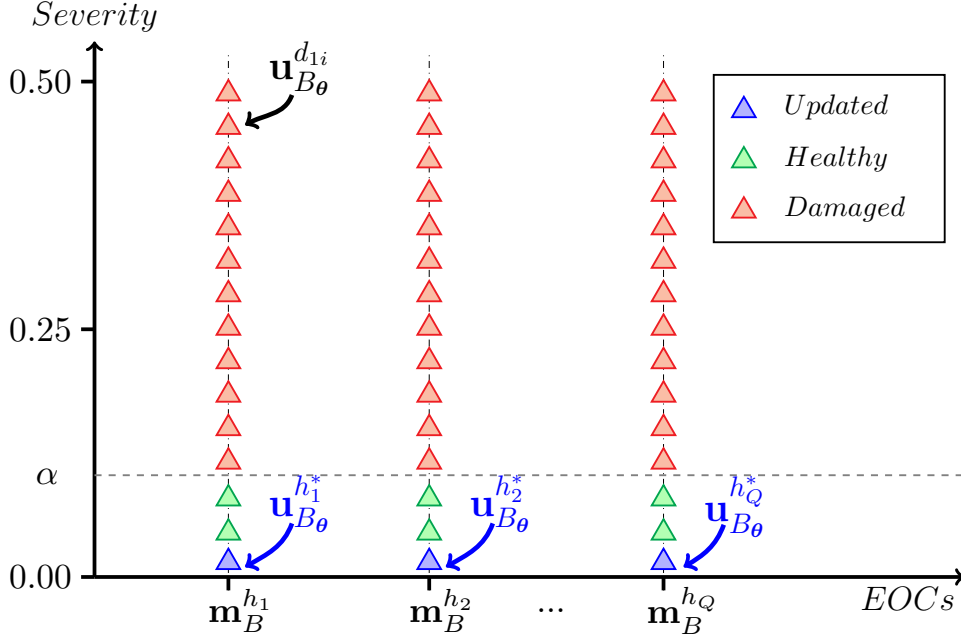
The relationship between the reduction factor

8

Figure 4: GMM-based synthetic database representation

and each severity level depends on the type of structural property. We distinguish material properties (type a), and boundary conditions (type b). The distinction is required given the different sensitivity of the dynamic response. For type a properties, we calculate the reduction factor as:

$$s_{i,j} = 1 - \alpha_{i,j} \qquad j = 1, .., n_{\theta_i}^a, \qquad (7)$$

where $s_{i,j}$ indicates the property damage severity, and $n_{\theta_i}^a$ indicates the number of a-type properties at the i-th location. We employ a different scale for type-b properties to induce damage in the structure effectively. We define the relationship between the reduction factor and its corresponding severity level as:

$$s_{i,j} = \frac{s_{max}}{\log_{10}(l_{i,j})} \log_{10}(\alpha_{i,j}) \qquad j = 1, ..., n_{\theta_i}^b, \quad (8)$$

where $n_{\theta_i}^b = n_{\theta_i} - n_{\theta_i}^a$ and $l_{i,j}$ represent the $j-th$ element in the lower bound vector $\mathbf{l}_i$. The expression in equation 8 is adequate for properties such as stiffness at supports (boundary conditions) given its large order of magnitude and the relative sensitivity of the structural response.

We now calculate the damage severity at the affected location as:

$$S_{B_\theta} = \mathcal{G}(\boldsymbol{\theta}_i) = \sqrt{\frac{1}{n_{\theta_i}} \sum_{j=1}^{n_{\theta_i}} s_{i,j}^2}, \qquad (9)$$

with $s_{i,j}$ representing the individual severity values for each property in the i-th zone, which are defined

9

next.

2.5. Database generation

We now build the synthetic database with damaged scenarios obtained under different EOCs corresponding to the Q representative measurements. For explanation purposes, we particularize to the i-th zone, but the methodology is extensible to all the n_z zones. We uniformly sweep the severity interval through an iterative process. For each scenario, we first generate a severity value S_{B_θ} by sampling from a uniform distribution: $S_{B_\theta} \sim \mathcal{U}(s_{min}, s_{max})$. S_{B_θ} is the target value to achieve with the individual severity values of each property at the damaged location using equation (9). We then obtain random values for the individual severity at each property according to a uniform distribution: $\bar{s}_{i,j} = rand(\mathcal{U}(0, s_{max}))$, with $j = 1, ..., n_{\theta_i}$. We calculate the prior severity level $\bar{S}$ by replacing $\bar{s}_{i,j}$ in equation (9). We subsequently correct the individual severity values to produce the target severity S by applying:

$$\mathbf{s}_i = \frac{S}{\bar{S}}\bar{\mathbf{s}}_i. \qquad (10)$$

We obtain the reduction vector $\boldsymbol{\alpha}_i$ from equations (7) and (8). In case any value in $\boldsymbol{\alpha}_i$ exceeds the admissible interval $[\mathbf{l}_i, 1)$, we generate a new set of individual severity values $\bar{\mathbf{s}}_i$ and recalculate $\boldsymbol{\alpha}_i$. We repeat this step until the constraint condition holds for all the reduction factors in the set. We finally calculate the damaged properties as $\boldsymbol{\theta}_i^d = \boldsymbol{\alpha}_i\boldsymbol{\theta}_i^*$. We describe the damaged bridge

parameterization by $B_\theta^d = \{\boldsymbol{\theta}_1^*, ..., \boldsymbol{\theta}_i^d, ..., \boldsymbol{\theta}_{n_z}^*\}$.

We follow this procedure to obtain n samples at the i-th zone. Thus, we produce $N = n_z \times n$ scenarios for each of the Q calibrated parametrizations. For each scenario, we calculate the dynamic responses by solving the eigenproblem:

$$\mathbf{u}_{B_\theta}^{(k)} = \mathcal{F}\left(B_\theta^{d_k}\right) \qquad k = 1, ..., N \qquad (11)$$

The k-th sample includes the dynamic response $\mathbf{u}_{B_\theta}^{(k)} = \{\mathbf{f}_{B_\theta}^{(k)}, \boldsymbol{\phi}_{B_\theta}^{(k)}\}$ and the corresponding damage condition label $\mathbf{D}_{B_\theta}^{(k)} = \{L_{B_\theta}^{(k)}, S_{B_\theta}^{(k)}\}$.

2.6. Two-step damage assessment

The final goal of this methodology is to estimate the true bridge condition (D_B). In this work, we employ DNNs to approximate the inverse problem ($\mathcal{I}$), such that:

$$D_B \approx \mathcal{I}_{\boldsymbol{\gamma}}(\mathbf{m}_B; \boldsymbol{\gamma}), \qquad (12)$$

where $\mathcal{I}_{\boldsymbol{\gamma}}$ denotes to the DNN and $\boldsymbol{\gamma}$ contains the network parameters. Training the DNN consists of finding the optimal network parameters to approximate the target function [37]. We define a loss function that measures the discrepancy between the predicted damage condition $\mathcal{I}_{\boldsymbol{\gamma}}(\mathbf{m}_B; \boldsymbol{\gamma})$ and the real state $\mathbf{D}_B$ employing the l_2 norm:

$$\mathcal{L}_{\boldsymbol{\gamma}} = \|\mathcal{I}_{\boldsymbol{\gamma}}(\mathbf{m}_B; \boldsymbol{\gamma}) - \mathbf{D}_B\|_2 \qquad (13)$$

During training, we find the optimal network parameters by solving the following minimization

10

problem:

$$\gamma^* := \arg\min_{\gamma}(\mathcal{L}_\gamma). \qquad (14)$$

Here, we propose a two-step approach to assess the bridge condition in terms of damage severity and location.

2.6.1. Damage severity estimation

We employ a DNN to estimate the damage severity, denoted by DNN_S. For the training stage of DNN_S, we include the available long-term monitoring data, M_B, which belong to the healthy state of the bridge. We assume that all the scenarios in M_B correspond to a severity value of $S = 0$, whereas the location label is unknown. These measurements contribute to learning different healthy states and preventing false positives. We then enrich M_B with the synthetic database of damage scenarios previously generated in section 2.1. We define the loss function $\mathcal{L}_\gamma^S$ according to equation (13), where the inverse operator $\mathcal{I}_\gamma$ refers to DNN_S, and the damage condition is the severity level: $D_B = S$.

Once trained, DNN_S receives new measured data from the monitoring system and provides a damage severity diagnostic. If the estimated severity for a specific measurement exceeds the predefined threshold α, we assume that damage exists and raise an alert.

2.6.2. Damage location estimation

After detecting and quantifying the damage, a subsequent DNN (DNN_L) receives the measurement to indicate its location. We only train DNN_L

with damaged samples from the database, i.e., those with a severity level $S \geq \alpha$. We define the loss function $\mathcal{L}_\gamma^L$, where $\mathcal{I}_\gamma$ refers to DNN_L with the damage condition being the location ($D_B = L$). This methodology prevents healthy scenarios from contributing to the location estimation during training since they could mislead the diagnostic. Figure 5 shows a flowchart of the proposed approach.

3. Numerical Results

We apply the proposed methodology to the case study of the Infante Dom Henrique bridge, considering three years of long-term dynamic monitoring data. We introduced the monitoring system in [59], and it is fully described in [67]. Figure 6 depicts the location of the acceleration sensors along the bridge deck. Four vertical acceleration signals are employed to calculate the dynamic properties (eigenfrequencies and eigenmodes) every 30 minutes through an automatic OMA technique [66]. Any measurement in M_B includes $v = 32$ variables: $n_m = 4$ eigenfrequencies and corresponding eigenmodes. We obtain seven-dimensional eigenmodes by fitting a spline to the four measurements and estimating the intermediate value between every two sensors. After removing null values, M_B contains a total of $N_m = 17,141$ samples.

3.1. GMM-based database

Given the high dimensionality of the dataset, we first apply Principal Component Analysis (PCA) to
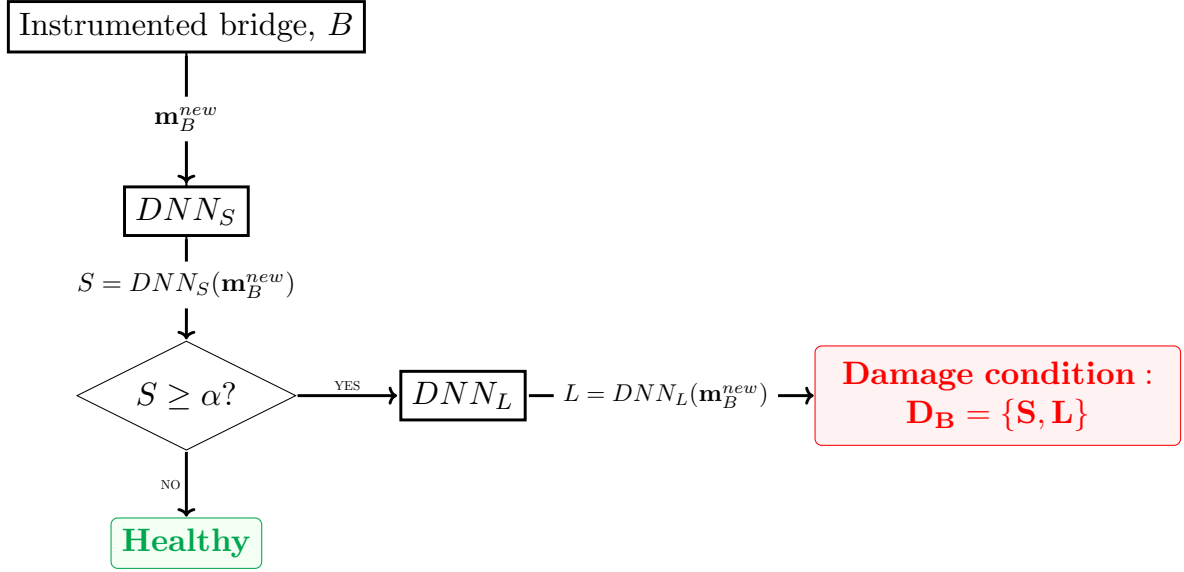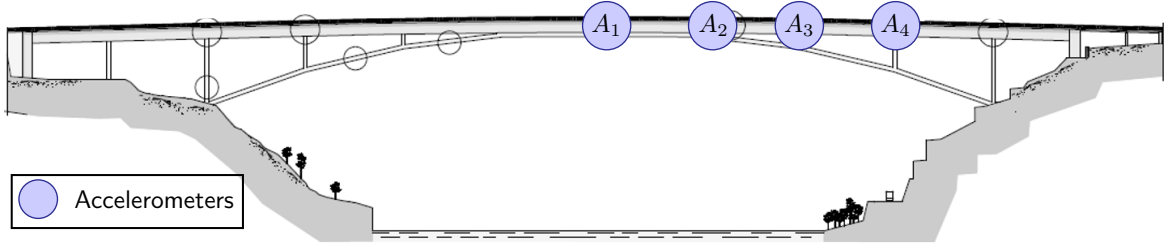
11

Figure 5: two-step assessment flowchart

Figure 6: Dynamic instrumentation system at Infante Dom Henrique bridge

compress the data and obtain relevant features for the clustering. Table 1 analyzes the explained variance for the first four principal components. The table reveals that the first PC explains most of the variance in the data, whereas the rest explains a residual part ($< 5\%$). We compress the original measurements into one-dimensional features by transforming them as:

$$\hat{M}_B = TM_B, \qquad (15)$$

where the transformation matrix T contains PC_1 coordinates.

We apply the GMM clustering technique to the transformed dataset $\hat{M}_B$.

We would ideally cluster the data into thousands of groups to include the entire EOC variability, but using a large number of clusters conflicts with the computational cost of obtaining the synthetic scenarios. With the available computational resources (Intel(R) Core(TM) i7-7700HQ, CPU 2.80GHz), each simulation executes in approximately 1.5 seconds. Thus, for the considered battery of damage

Table 1: Principal Component Analysis results

	$\mathbf{PC}_1$	$\mathbf{PC}_2$	$\mathbf{PC}_3$	$\mathbf{PC}_4$
Explained Variance (%)	95.55	1.80	0.92	0.72
Cumulated (%)	95.55	97.35	98.27	98.99

scenarios, each cluster adds approximately 17 hours of computational time, including (i) the FEMU calibration step and (ii) the generation of the damage scenarios.

We explore the clustering error by analyzing the log-likelihood metric for an increasing number of clusters, Q [68]. This score function founds on the likelihood, which measures the probability that the available data X was generated from the model [69]. The value of this metric depends on the data amplitude and lacks meaningful interpretation, but it is useful for performance comparison. For the GMM model, we calculate the log-likelihood $l(\boldsymbol{\phi}|X)$ as:

$$l(\boldsymbol{\phi}|X) = \sum_{i=1}^{N} log(\sum_{q=1}^{Q} \pi_q \mathcal{N}(x_i|\mu_q, \Sigma_q)), \qquad (16)$$

with $\boldsymbol{\phi} = \{\pi_1, ..., \pi_Q, \mu_1, ..., \mu_Q, \Sigma_1, ..., \Sigma_Q\}$ gathering the mixture parameters, and N being the number of data samples in X. Figure 7 displays the log-likelihood value for mixtures with Q in the interval $[2, 8]$. We observe that the most significant improvement occurs between $Q = 2$ and $Q = 4$, whereas after $Q = 6$, the enhancement is unnoticeable. Based on this and given that we aim to include most of the variability in the data but with the computational restriction, we decide to
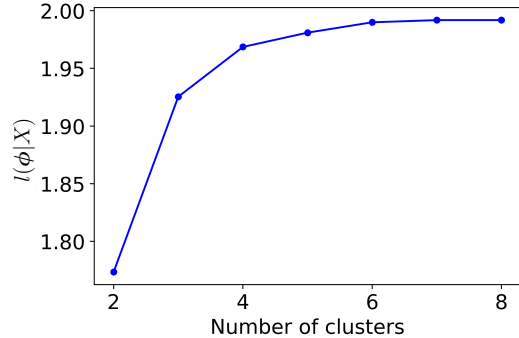

Figure 7: Log-likelihood metric for increasing Q

employ five clusters ($Q = 5$). This decision results in $17 \times 5 = 85$ hours to build the database.

Table 2 presents the five mean values of the gaussians. Figure 8b displays the transformed dataset $\hat{M}_B$ colored by cluster label. Figure 8a shows the distribution of the samples in the Q clusters. According to Figure 8b, we appreciate that the data dispersion increases with the value of the PCA transformation feature. Cluster four contains only 54 samples very widely spread, indicating that they could be outliers. However, the analysis of these data is out of the scope of this work.

After performing the clustering, we obtain the five points in the transformed space that lie closer to the means according to equation (3). Finally, we extract the corresponding 32-dimensional measurements: $M_B^{GMM} = \{\mathbf{m}_B^{h_0}, \mathbf{m}_B^{h_1}, \mathbf{m}_B^{h_2}, \mathbf{m}_B^{h_3}, \mathbf{m}_B^{h_4}\}$. For each of these five measurements, we solve the

13

Table 2: Mean vector coordinates for the five clusters

	$\boldsymbol{\mu}_0$	$\boldsymbol{\mu}_1$	$\boldsymbol{\mu}_2$	$\boldsymbol{\mu}_3$	$\boldsymbol{\mu}_4$
Value	-1.3867	-1.3112	-1.1325	-0.8167	0.0024
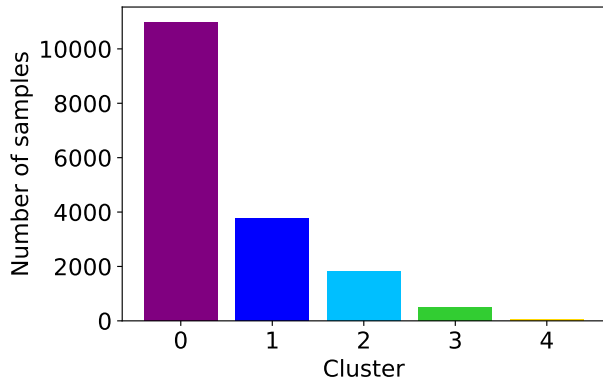
(a) Samples distribution.
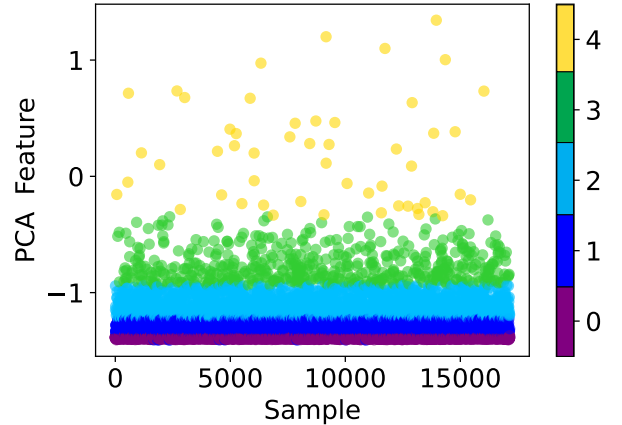
(b) Dataset clustering.

Figure 8: Dataset clustering results for $Q = 5$.

Finite Element Model Updating (FEMU) process to obtain the calibrated parametrizations, yielding the responses $U_{B_{\boldsymbol{\theta}}}^{GMM} = \{\mathbf{u}_{B_{\boldsymbol{\theta}}}^{h_0^*}, \mathbf{u}_{B_{\boldsymbol{\theta}}}^{h_1^*}, \mathbf{u}_{B_{\boldsymbol{\theta}}}^{h_2^*}, \mathbf{u}_{B_{\boldsymbol{\theta}}}^{h_3^*}, \mathbf{u}_{B_{\boldsymbol{\theta}}}^{h_4^*}\}$.

We generate the synthetic scenarios and conform the new database following the steps in section 2.5. We generate a total of $N_s = 80,000$ synthetic samples containing damage scenarios: $n_s = 2,000$ samples for each of the $n_z = 8$ zones in the bridge and for each of the five responses in $U_{B_{\boldsymbol{\theta}}}^{GMM}$. The computational time of generating this database is of approximately 85 hours (including the FEMU step). The entire database contains $N = N_m + N_s = 97,141$ samples, including the healthy experimental measurements and the synthetic samples that include the damage scenarios.

3.2. Deep Neural Networks for a two-step assessment

Here, we employ fully-connected feedforward DNNs with ReLU[37] activation functions in the hidden layers. We employ the complete response as the input (the four eigenfrequencies and eigenmodes). Thus, each sample contains $v = 32$ dimensions. Table 3 summarizes the properties of the Deep Neural Networks. The architectures provide adequate performance. Optimizing the architectures is out of the scope of this research.

We first train the severity estimator DNN_S. We randomly split the available data (N samples) into 70% for training, 20% for validation, and 10% for testing. We evaluate the performance of the network with the validation dataset. Figure 9a shows the severity cross-plot that compares the ground

Table 3: Summary of architecture and training specifications

ID	Hidden Layers	Parameters	Optimizer	Batch size	LR
DNN_S	9	36,597	Adam	8,196	10^{-4}
DNN_L	6	7,879	Adam	8,196	10^{-4}

truth against the estimated severity values. The figure shows a high-prediction performance with the r^2 metric reaching 0.96. We follow the same procedure for the location estimator, DNN_L. In this case, we restrict the training data to those scenarios where $S > \alpha$, with $\alpha = 0.05$ indicating the lowest detectable damage. Figure 9b shows the corresponding cross-plot that compares the ground truth against the estimated location values. The figure shows an adequate approximation of DNN_L given the high correlation factor during validation.

3.3. Synthetic testing

Here, we analyze the methodology in the task of damage identification. Since real damage scenarios are unavailable in full-scale operative bridge applications, we employ synthetic damage cases for testing.

We aim to analyze the enhancement of the proposed methodology with respect to the original approach described in our previous work [59] in damage identification. For the comparison, we generate a database according to Figure 1 that disregards the effect of changing EOCs. Given that cluster zero is the most significative in M_B according to Figure 8a, we employ $\mathbf{m}_B^{h_0}$ as the baseline healthy measurement to build the database. Hence, the original database contains the synthetic scenarios generated from $\mathbf{u}_{B\boldsymbol{\theta}}^{h_0^*}$. We denote $DNN_S^{original}$ and $DNN_L^{original}$ to the neural networks described in section 3.2 trained with the original database.

3.3.1. Synthetic testing under seen EOCs

We first evaluate the damage detection performance for scenarios occurring under the same EOCs considered during training. This testing dataset corresponds to 10% of the available samples according to the database splitting (70% training, 20% validation, and 10% testing).

(A) Performance of the original approach: Here, we test the damage identification ability of the original database created from $\mathbf{u}_{B\boldsymbol{\theta}}^{h_0^*}$. In this case, the testing subset contains damage scenarios occurring only under the particular EOCs of $\mathbf{m}_B^{h_0}$.

We first evaluate $DNN_S^{original}$ to estimate the severity of the damage. Figure 10a shows the corresponding cross-plot that displays the ground truth (real severity label) against the prediction provided by DNN_S. The squared correlation coefficient ($r^2 \approx 0.94$) indicates a high performance. We subsequently estimate the location of the damage. Figure 10b displays the location cross-plot. $DNN_L^{original}$ also reveals an extraordinary performance during this test ($r^2 \approx 0.94$).
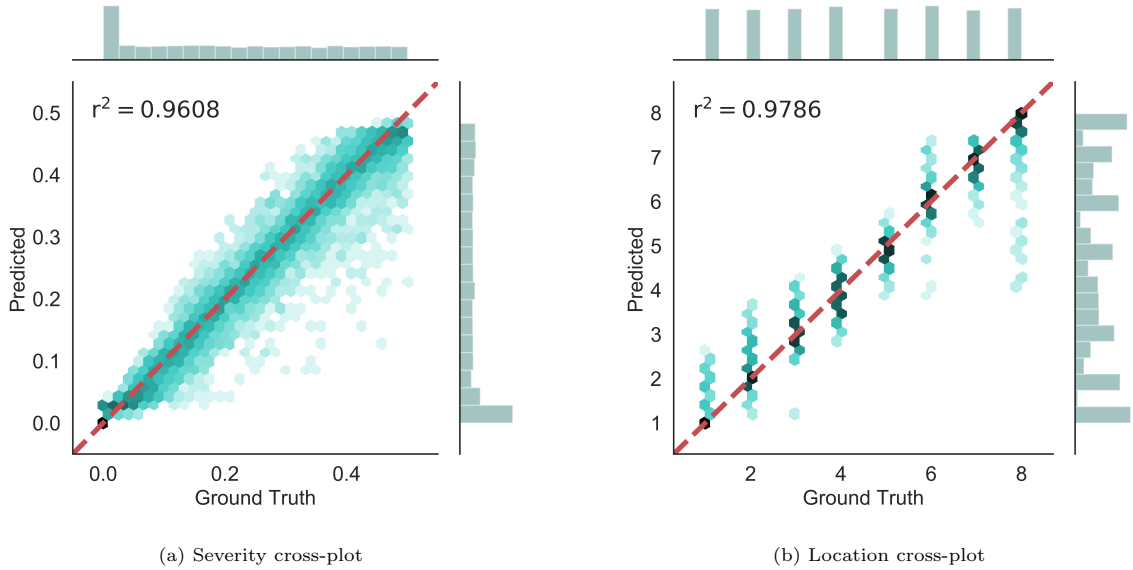
(a) Severity cross-plot

(b) Location cross-plot

Figure 9: DNN_S and DNN_L cross-plots during validation

(B) Performance of the GMM-based method: We now test the damage identification ability of the new proposed database. This database contains synthetic scenarios generated from the updated parametrizations with responses stored in $U_{B_{\boldsymbol{\theta}}}^{GMM}$. Hence, the testing damage scenarios are assumed to occur under the same EOCs of the five corresponding measurements in M_B^{GMM}.

We evaluate DNN_S to estimate the severity of the damage. Figure 11a shows the resulting cross-plot. The squared correlation coefficient indicates a good performance with $r^2 \approx 0.94$. We subsequently estimate the damage location for those scenarios exceeding the threshold α. Figure 11b displays the cross-plot, revealing a very high performance of DNN_L ($r^2 \approx 0.98$). These results demonstrate that the proposed two-step DNN assessment adequately performs as good as the original approach

when damage occurs under the same EOCs employed during training.

3.3.2. Synthetic testing under unseen EOCs

We now investigate the performance of the methodology for damage scenarios occurring under different EOCs unseen during the training phase. This test evaluates if applying GMM to select representative measurements for the training database contributes to generalizing the damage assessment task under different (unseen) EOCs.

We first select three test measurements from the monitoring data M_B that belong to three different clusters, denoted by $\{\mathbf{m}_B^{t_1}, \mathbf{m}_B^{t_2}, \mathbf{m}_B^{t_3}\}$. We employ only three measurements to restrict the computational cost required by the entire methodology. According to the clustering results in Figure 8a, we extract the measurements from the most relevant (highest-occurrence frequency) clus-

ters, namely, zero, one, and two. Table 4 summarizes the main properties of these measurements, including the value of the four eigenfrequencies, the PCA compressed feature, and the cluster label.

We solve the FE model updating process to obtain the calibrated parametrizations, yielding the responses $U_{B_{\boldsymbol{\theta}}}^{Test} = \{\mathbf{u}_{B_{\boldsymbol{\theta}}}^{t_1^*}, \mathbf{u}_{B_{\boldsymbol{\theta}}}^{t_2^*}, \mathbf{u}_{B_{\boldsymbol{\theta}}}^{t_3^*}\}$. We then generate $n_t = 50$ synthetic scenarios with random severity within the interval $[0, 0.5]$ for each of the $n_z = 8$ zones in the bridge. The testing dataset contains a total of $1,200$ samples (400 for each parametrization in $U_{B_{\boldsymbol{\theta}}}^{Test}$). Figure 12 shows a representative example of the testing samples for one of the bridge zones with $n_t = 8$ synthetic scenarios. The figure evidences that the testing EOCs differ from those considered during training.

(A) Performance of the original approach: We evaluate the performance of the original database generated from $\mathbf{m}_B^{h_0}$. Figure 13 shows the cross-plots for severity and location.

Figure 13a reveals that this approach fails to detect damage, with an overall score $r^2 \approx 0.37$. We observe that points from cluster zero present better estimations than those belonging to clusters one and two. This result demonstrates that neglecting changes in EOCs during training misleads the assessment under different conditions. In the case of location, we also observe poor predictions from $DNN_L^{original}$, evidencing the unreliability of neglecting EOCs.

(B) Performance of the proposed GMM-based method: We finally evaluate the performance of the GMM-based methodology under changing EOCs. Figure 14a shows the severity cross-plot. The squared correlation coefficient indicates an adequate performance with $r^2 \approx 0.85$. We subsequently estimate the damage location for the scenarios with $S \geq \alpha$. Figure 14b displays the corresponding cross-plot. We also observe an adequate performance of DNN_L, with $r^2 \approx 0.85$. The color clasification based on clusters prevents showing clearly the density of points concentrating around the exact estimator (predicted = ground truth), but the r^2 value demonstrates the good performance. These results reveal that the proposed methodology gains robustness against the effect of varying EOCs during assessment. If more computational resources were available, we would consider a higher number of clusters to produce a more representative database that further enhances performance.

4. Discussion

This work employs synthetic measurements simulated with a FE model. Building a FE model requires assumptions and simplifications that introduce a new source of uncertainty and error. In work [26], the authors explore the effect of modeling error and uncertainty in the updating process for damage assessment. Sources of uncertainty are the assumptions and simplifications due to a lack of knowledge of the true system's behavior, in-

Table 4: Summary of selected testing points

Case	f_1	f_2	f_3	f_4	PCA feature	Cluster
$\mathbf{m}_B^{t_1}$	0.8121	1.1426	1.4123	2.0049	-1.3825	0
$\mathbf{m}_B^{t_2}$	0.8165	1.1491	1.4189	2.0184	-1.2678	1
$\mathbf{m}_B^{t_3}$	0.8172	1.1429	1.4064	1.9998	-1.1644	2

cluding material properties or boundary conditions [26]. The discretization level in FE parametrizations also introduces a source of error. There exist many works in the literature concerned with this problem [26, 70, 71, 60]. For example, work [72] analyzes the effect of these modeling errors in the prediction results of a Convolutional DNN trained with FE simulations of a lab-scale truss bridge. Work [73] deals with the uncertainty of using simplified Frequency Response Function (FRF) data as the damage-sensitive input feature to train a DNN. In the recent work [74], authors employ a physics-guided NN method to reduce the effect of uncertainty and modeling error in the damage identification task under vehicle-induced excitation.

In our approach, we design a relatively simple FE model with a rough parametrization and assume that, after the FEMU process, it will deliver a close enough approximation to the target experimental response. Some uncertainties in material properties and simplifications in modeling pier and abutment connections are present. We expect these errors to be sufficiently small compared to the effect of damage. The lack of experimental damage scenarios precludes a real validation of the SHM methodology in damage identification. Our validation focuses on evaluating the Deep Neural Networks for new synthetic scenarios corresponding to particular EOCs different from those employed during training. However, this strategy overlooks the effect of modeling errors and uncertainties mentioned above. The absence of real damage occurs in most full-scale applications, with very few exceptions in the civil engineering field, such as the Z24 benchmark case study [75, 57].

Another critical aspect when using synthetic data is incorporating the effect of varying EOCs. Many works employing model-based assessment neglect the effect of varying EOCs and focus on deterministic FEMU techniques [15, 16, 17, 18, 19, 20]. Work [21] studies the effect of changing EOCs in standard FEMU and reveals that uncertainty propagates through the updating procedure, yielding wrong state identifications. In [71], the authors incorporate ambient temperature and wind effect in the iterative updating process. Our work intends to embed information from the experimental domain into the synthetic scenarios using representative experimental measurements as the target response to solve FEMU problems before generating the damage scenarios. However, it presents a limitation regarding the computational cost associated

with solving many FE simulations, which constrains the decision on the extent of the database. For the considered full-scale case study, each additional measurement adds 17 computation hours, forcing us to select a reduced number (five) of representative measurements. For more accurate results in damage identification under any EOCs, we need to extend the database to incorporate these phenomena.

5. Conclusions and future work

In this work, we addressed a hybrid SHM approach that combines model-based and data-driven techniques to identify damage in bridge structures. Starting from the hybrid methodology developed in our previous work [59], we realized that neglecting the effect of EOCs might have detrimental consequences in the health diagnostic. We proposed a novel approach to enhance the assessment capability by incorporating varying EOCs in the synthetic damage scenarios. We applied a Gaussian Mixture clustering technique to extract Q representative measurements from a long-term monitoring campaign corresponding to specific EOCs. These measurements constituted the target responses to update a FE parametrization and represent Q different undamaged conditions. With these calibrated models, we generated multiple synthetic scenarios labeled by damage severity and location. We employed a two-step Deep Learning approach to evaluate the damage condition: once a new response is measured, a DNN (DNN_S) first estimates the damage severity. If the estimation exceeds a predefined threshold, then a second DNN (DNN_L) receives the measurement to determine the damage location.

We applied the proposed methodology to the Infante Dom Henrique bridge in Porto. During testing, we compared the assessment performance of our approach against the original one introduced in [59], where we employed one single measurement in the synthetic database generation step. The analysis of the obtained results confirms that neglecting the presence of varying EOCs in real-practice SHM applications prevents achieving an adequate assessment. Although both methodologies are robust in detecting and locating damage occurring under the same EOCs considered in the training phase, the original approach fails when tested under different EOCs. Including more measurements extracted from long-term monitoring data in the database generation process enhances the method performance and allows generalizing the assessment to a wide range of EOCs.

Given the limitation derived from the computational cost of including more measurements in the database generation, we consider future work a more profound investigation for a more effective measurement selection. We can optimize the number of clusters and determine the number of extracted measurements per group according to the cluster population and dispersion. Besides, many

uncertainty and error sources coexist in this hybrid approach, arising from the measurements and the FE parametrization (simplifications and assumptions on the structural behavior). We consider future work using Bayesian approaches to leverage these uncertainties in the FEMU process and obtain more reliable parametrizations. In terms of assessment, endowing the DNNs with a Bayesian scope may enhance the robustness of the diagnostic by quantifying the uncertainty. Using physics-guided approaches to embedding structural knowledge during training poses a new line of interest to investigate.

Finally, we also contemplate as future work transferring the methodology to other application areas, such as offshore wind energy structures, where complex environmental and operational conditions hold, and late maintenance and repair tasks have a high economic impact.

References

[1] C. Farrar, K. Worden, Structural Health Monitoring A Machine Learning Perspective, Wiley, 2013. doi:10.1002/9781118443118.

[2] A. Rytter, Vibrational based inspection of civil engineering structures, Ph.D. thesis, University of Aalborg, Denmark, ph.D.-Thesis defended publicly at the University of Aalborg, April 20, 1993 PDF for print: 206 pp. (1993).

[3] S. Teng, G. Chen, Z. Liu, L. Cheng, X. Sun, Multi-sensor and decision-level fusion-based structural damage detection using a one-dimensional convolutional neural network, Sensors 21 (2021). doi:10.3390/s21123950.

[4] Y. Ding, A. Li, Assessment of bridge expansion joints using long-term displacement measurement under changing environmental conditions, Frontiers of Architecture and Civil Engineering in China 5 (3) (2011) 374–380. doi:10.1007/s11709-011-0122-x.

[5] C. K. Oh, H. Sohn, I. H. Bae, Statistical novelty de-

tection within the Yeongjong suspension bridge under environmental and operational variations, Smart Materials and Structures 18 (12) (2009). doi:10.1088/0964-1726/18/12/125022.

[6] H. Sohn, Effects of environmental and operational variability on structural health monitoring-doi:10.1098/rsta.2006.1935.

[7] E. Reynders, G. Wursten, G. de Roeck, Output-only structural health monitoring in changing environmental conditions by means of nonlinear system identification, Structural Health Monitoring 13 (1) (2014) 82–93. arXiv:arXiv:1210.2490v1, doi:10.1177/1475921713502836.

[8] C. Rainieri, F. Magalhaes, Challenging aspects in removing the influence of environmental factors on modal parameter estimates, Procedia Engineering 199 (2017) 2244 – 2249, x International Conference on Structural Dynamics, EURODYN 2017. doi:https://doi.org/10.1016/j.proeng.2017.09.210.

[9] Y. Shokrani, V. K. Dertimanis, E. N. Chatzi, M. N. Savoia, On the use of mode shape curvatures for damage localization under varying environmental conditions, Structural Control and Health Monitoring 25 (4) (2018). doi:10.1002/stc.2132.

[10] Y. An, E. Chatzi, S. H. Sim, S. Laflamme, B. Blachowski, J. Ou, Recent progress and future trends on damage identification methods for bridge structures (oct 2019). doi:10.1002/stc.2416.
URL https://onlinelibrary.wiley.com/doi/abs/10.1002/stc.2416

[11] P. Cawley, Structural health monitoring: Closing the gap between research and industrial deployment, Structural Health Monitoring 17 (5) (2018) 1225–1244. doi:10.1177/1475921717750047.

[12] H.-P. Chen, Y.-Q. Ni, Structural Damage Identification Techniques, John Wiley and Sons, Ltd, 2018, Ch. 4, pp. 69–90. doi:https://doi.org/10.1002/9781119166641.ch4.

[13] M. I. Friswell, J. E. Mottershead, Finite Element Model Updating in Structural Dynamics, Vol. 38 of Solid Mechanics and its Applications, Springer Netherlands, Dordrecht, 1995. doi:10.1007/978-94-015-8508-8.

[14] M. I. Friswell, Damage identification using inverse methods, Philosophical Transactions of the Royal Society A: Mathematical, Physical and Engineering Sciences 365 (1851) (2007) 393–410. doi:10.1098/rsta.2006.1930.

[15] J. R. Wu, Q. S. Li, Finite element model updating for a high-rise structure based on ambient vibration measurements, Engineering Structures 26 (7) (2004) 979–990. doi:10.1016/j.engstruct.2004.03.002.

[16] T. Liu, Q. Zhang, T. Zordan, B. Briseghella, Finite Element Model Updating of Canonica Bridge Using Experimental Modal Data and Genetic Algorithm, Structural Engineering International 26 (1) (2016) 27–36. doi:10.2749/101686616X14480232444405.

[17] S. Schommer, V. H. Nguyen, S. Maas, A. Zürbes, Model updating for structural health monitoring using static and dynamic measurements, in: Procedia Engineering, Vol. 199, 2017, pp. 2146–2153. doi:10.1016/j.proeng.2017.09.156.

[18] W. Petersen, O. Øiseth, Sensitivity-based finite element model updating of a pontoon bridge, Engineering Structures 150 (2017) 573–584. doi:10.1016/j.engstruct.2017.07.025.

[19] N. Grip, N. Sabourova, Y. Tu, Sensitivity-based model updating for structural damage identification using total variation regularization, Mechanical Systems and Signal Processing 84 (51378104) (2017) 365–383. arXiv:1602.08137, doi:10.1016/j.ymssp.2016.07.012.

[20] H. Tran-Ngoc, S. Khatir, G. De Roeck, T. Bui-Tien, L. Nguyen-Ngoc, M. Abdel Wahab, Model Updating for Nam O Bridge Using Particle Swarm Optimization Algorithm and Genetic Algorithm, Sensors 18 (12) (2018) 4131. doi:10.3390/s18124131.
URL http://www.mdpi.com/1424-8220/18/12/4131

[21] B. Moaveni, I. Behmanesh, Effects of changing ambient temperature on finite element model updating of the Dowling Hall Footbridge, Engineering Structures 43

(2012) 58–68. doi:10.1016/j.engstruct.2012.05.009.

URL http://dx.doi.org/10.1016/j.engstruct.2012.05.009

[22] M. Song, I. Behmanesh, B. Moaveni, C. Papadimitriou, Accounting for modeling errors and inherent structural variability through a hierarchical bayesian model updating approach: An overview, Sensors 20 (14) (2020).

[23] X. Jia, O. Sedehi, C. Papadimitriou, L. Katafygiotis, B. Moaveni, Two-stage hierarchical bayesian framework for finite element model updating, 2020.

[24] T. Dalgleish, J. M. G. Williams, A.-M. J. Golden, N. Perkins, L. F. Barrett, P. J. Barnard, C. Au Yeung, V. Murphy, R. Elward, K. Tchanturia, E. Watkins, Probabilistic Finite Element Model Updatin using Bayesian Statistics, Vol. 136, 2007.

[25] P. Asadollahi, Y. Huang, J. Li, Bayesian finite element model updating and assessment of cable-stayed bridges using wireless sensor data, Sensors (Switzerland) 18 (9) (2018). doi:10.3390/s18093057.

[26] E. Simoen, G. De Roeck, G. Lombaert, Dealing with uncertainty in model updating for damage assessment: A review, Mechanical Systems and Signal Processing 56 (2015) 123–149. doi:10.1016/j.ymssp.2014.11.001.

URL http://dx.doi.org/10.1016/j.ymssp.2014.11.001

[27] Y. An, E. Chatzi, S.-H. Sim, S. Laflamme, B. Blachowski, J. Ou, Recent progress and future trends on damage identification methods for bridge structures, Structural Control and Health Monitoring 26 (10) (2019) e2416, e2416 STC-18-0435.R3. doi:https://doi.org/10.1002/stc.2416.

[28] D. Giagopoulos, A. Arailopoulos, V. Dertimanis, C. Papadimitriou, E. Chatzi, K. Grompanopoulos, Structural health monitoring and fatigue damage estimation using vibration measurements and finite element model updating, Structural Health Monitoring 18 (4) (2019) 1189–1206. doi:10.1177/1475921718790188.

[29] A. Kamariotis, E. Chatzi, D. Straub, Value of information from vibration-based structural health monitoring extracted via bayesian model updating, Mechanical Systems and Signal Processing 166 (2022) 108465.

doi:https://doi.org/10.1016/j.ymssp.2021.108465.

[30] S. Mustafa, N. Debnath, A. Dutta, Bayesian probabilistic approach for model updating and damage detection for a large truss bridge, International Journal of Steel Structures 15 (2) (2015) 473–485. doi:10.1007/s13296-015-6016-3.

[31] T. Marwala, Finite Element Model Updating Using Computational Intelligence Techniques: Applications to Structural Dynamics, Springer, 2010. doi:10.1007/978-1-84996-323-7.

[32] S. Qin, Y. L. Zhou, H. Cao, M. A. Wahab, Model Updating in Complex Bridge Structures using Kriging Model Ensemble with Genetic Algorithm, KSCE Journal of Civil Engineering 22 (9) (2018) 3567–3578. doi:10.1007/s12205-017-1107-7.

[33] E. García-Macías, L. Ierimonti, I. Venanzi, F. Ubertini, An innovative methodology for online surrogate-based model updating of historic buildings using monitoring data, International Journal of Architectural Heritage 15 (1) (2021) 92–112. doi:10.1080/15583058.2019.1668495.

[34] C. R. Farrar, S. W. Doebling, D. A. Nix, Vibration-based structural damage identification 359 (1778) (2001) 131–149. doi:10.1098/rsta.2000.0717.

[35] M. Gul, F. Necati Catbas, Statistical pattern recognition for Structural Health Monitoring using time series modeling: Theory and experimental verifications, Mechanical Systems and Signal Processing 23 (7) (2009) 2192–2204. doi:10.1016/j.ymssp.2009.02.013.

URL http://dx.doi.org/10.1016/j.ymssp.2009.02.013

[36] O. Avci, O. Abdeljaber, S. Kiranyaz, M. Hussein, M. Gabbouj, D. J. Inman, A review of vibration-based damage detection in civil structures: From traditional methods to Machine Learning and Deep Learning applications, Mechanical Systems and Signal Processing 147 (2021) 107077. doi:10.1016/j.ymssp.2020.107077.

URL https://doi.org/10.1016/j.ymssp.2020.107077

[37] I. Goodfellow, Y. Bengio, A. Courville, Deep Learning, The MIT Press, 2016.

[38] M. Azimi, A. D. Eslamlou, G. Pekcan, Data-driven structural health monitoring and damage detection through deep learning: State-of-the-art review, Sensors 20 (10) (2020). doi:10.3390/s20102778.

[39] V. Meruane, W. Heylen, Structural damage assessment under varying temperature conditions, Structural Health Monitoring 11 (3) (2012) 345–357. doi:10.1177/1475921711419995.

[40] D. Sen, S. Nagarajaiah, Data-Driven Approach to Structural Health Monitoring Using Statistical Learning Algorithms (2018) 295–305.

[41] A. Bakdi, A. Kouadri, S. Mekhilef, A data-driven algorithm for online detection of component and system faults in modern wind turbines at different operating zones, Renewable and Sustainable Energy Reviews 103 (January 2018) (2019) 546–555. doi:10.1016/j.rser.2019.01.013.
URL https://doi.org/10.1016/j.rser.2019.01.013

[42] D. A. Tibaduiza, L. E. Mujica, J. Rodellar, A. Güemes, Structural damage detection using principal component analysis and damage indices, Journal of Intelligent Material Systems and Structures 27 (2) (2016) 233–248. doi:10.1177/1045389X14566520.

[43] A. Bellino, A. Fasana, L. Garibaldi, S. Marchesiello, PCA-based detection of damage in time-varying systems, Mechanical Systems and Signal Processing 24 (7) (2010) 2250–2260. doi:10.1016/j.ymssp.2010.04.009.
URL http://dx.doi.org/10.1016/j.ymssp.2010.04.009

[44] B. Peeters, J. Maeck, G. De Roeck, Vibration-based damage detection in civil engineering: Excitation sources and temperature effects, Smart Materials and Structures 10 (2001) 518. doi:10.1088/0964-1726/10/3/314.

[45] E. J. Cross, G. Manson, K. Worden, S. G. Pierce, Features for damage detection with insensitivity to environmental and operational variations, Proceedings of the Royal Society A: Mathematical, Physical and Engineering Sciences 468 (2012) 4098 – 4122.

[46] D. Garcia-Sanchez, A. Fernandez-Navamuel, D. Z. Sánchez, D. Alvear, D. Pardo, Bearing assessment tool for longitudinal bridge performance, Journal of Civil Structural Health Monitoring (2020) 1–25doi:10.1007/s13349-020-00432-1.

[47] M. Silva, A. Santos, R. Santos, E. Figueiredo, C. Sales, J. C. Costa, Deep principal component analysis: An enhanced approach for structural damage identification, Structural Health Monitoring 18 (5-6) (2019) 1444–1463. doi:10.1177/1475921718799070.

[48] A. Fernandez-Navamuel, F. Magalhães, D. Zamora-Sánchez, Ángel J Omella, D. Garcia-Sanchez, D. Pardo, Deep learning enhanced principal component analysis for structural health monitoring, Structural Health Monitoring 0 (0) (0) 14759217211041684. arXiv:https://doi.org/10.1177/14759217211041684, doi:10.1177/14759217211041684.
URL https://doi.org/10.1177/14759217211041684

[49] N. Dervilis, I. Antoniadou, R. J. Barthorpe, E. J. Cross, K. Worden, Robust methods for outlier detection and regression for SHM applications, International Journal of Sustainable Materials and Structural Systems 2 (1/2) (2015) 3. doi:10.1504/ijsmss.2015.078354.

[50] J. P. Santos, A. D. Orcesi, C. Crémona, P. Silveira, Baseline-free real-time assessment of structural changes, Structure and Infrastructure Engineering 11 (2) (2015) 145–161. arXiv:https://doi.org/10.1080/15732479.2013.858169, doi:10.1080/15732479.2013.858169.
URL https://doi.org/10.1080/15732479.2013.858169

[51] E. García-Macías, F. Ubertini, Mova/moss: Two integrated software solutions for comprehensive structural health monitoring of structures, Mechanical Systems and Signal Processing 143 (2020) 106830. doi:https://doi.org/10.1016/j.ymssp.2020.106830.

[52] T. Amarbayasgalan, B. Jargalsaikhan, K. H. Ryu, Unsupervised novelty detection using deep autoencoders with density based clustering, Applied Sciences (Switzerland) 8 (9) (2018). doi:10.3390/app8091468.

[53] Z. Zhang, C. Sun, Structural damage identifi-

cation via physics-guided machine learning: a methodology integrating pattern recognition with finite element model updating, Structural Health Monitoring 20 (4) (2021) 1675–1688. arXiv:https://doi.org/10.1177/1475921720927488, doi:10.1177/1475921720927488.
URL https://doi.org/10.1177/1475921720927488

[54] Z. Mousavi, M. M. Ettefagh, M. H. Sadeghi, S. N. Razavi, Developing deep neural network for damage detection of beam-like structures using dynamic response based on fe model and real healthy state, Applied Acoustics 168 (2020) 107402. doi:https://doi.org/10.1016/j.apacoust.2020.107402.

[55] P. Seventekidis, D. Giagopoulos, A. Arailopoulos, O. Markogiannaki, Structural health monitoring using deep learning with optimal finite element model generated data, Mechanical Systems and Signal Processing 145 (2020) 106972. doi:https://doi.org/10.1016/j.ymssp.2020.106972.

[56] C. S. N. Pathirage, J. Li, L. Li, H. Hao, W. Liu, P. Ni, Structural damage identification based on autoencoder neural networks and deep learning, Engineering Structures 172 (January) (2018) 13–28. doi:10.1016/j.engstruct.2018.05.109.
URL https://doi.org/10.1016/j.engstruct.2018.05.109

[57] E. Figueiredo, I. Moldovan, A. Santos, P. Campos, J. C. Costa, Finite Element-Based Machine-Learning Approach to Detect Damage in Bridges under Operational and Environmental Variations, Journal of Bridge Engineering 24 (7) (2019) 1–13. doi:10.1061/(ASCE)BE.1943-5592.0001432.

[58] P. Seventekidis, D. Giagopoulos, A combined finite element and hierarchical deep learning approach for structural health monitoring: Test on a pin-joint composite truss structure, Mechanical Systems and Signal Processing 157 (2021) 107735. doi:https://doi.org/10.1016/j.ymssp.2021.107735.

[59] A. Fernandez-Navamuel, D. Zamora-Sánchez, Ángel J. Omella, D. Pardo, D. Garcia-Sanchez, F. Ma-

galhães, Supervised deep learning with finite element simulations for damage identification in bridges, Engineering Structures 257 (2022) 114016. doi:https://doi.org/10.1016/j.engstruct.2022.114016.

[60] P. Seventekidis, D. Giagopoulos, A. Arailopoulos, O. Markogiannaki, Damage identification of structures through machine learning techniques with updated finite element models and experimental validations, in: Model Validation and Uncertainty Quantification, Volume 3, Springer International Publishing, Cham, 2020, pp. 143–154.

[61] Y. Liu, S. Zhang, Probabilistic Baseline of Finite Element Model of Bridges under Environmental Temperature Changes, Computer-Aided Civil and Infrastructure Engineering 32 (7) (2017) 581–598. doi:10.1111/mice.12268.

[62] A.-M. Yan, G. Kerschen, P. De Boe, J.-C. Golinval, Structural damage diagnosis under varying environmental conditions—part i: A linear analysis, Mechanical Systems and Signal Processing 19 (4) (2005) 847–864. doi:https://doi.org/10.1016/j.ymssp.2004.12.002.

[63] E. Patel, D. S. Kushwaha, Clustering cloud workloads: K-means vs gaussian mixture model, Procedia Computer Science 171 (2020) 158–167, third International Conference on Computing and Network Communications (CoCoNet'19). doi:https://doi.org/10.1016/j.procs.2020.04.017.

[64] M. P. Deisenroth, A. A. Faisal, C. S. Ong, Mathematics for Machine Learning, Cambridge University Press, 2020. doi:10.1017/9781108679930.

[65] J. Santos, C. Crémona, P. Silveira, Automatic operational modal analysis of complex civil infrastructures, Structural Engineering International 30 (3) (2020) 365–380. arXiv:https://doi.org/10.1080/10168664.2020.1749012, doi:10.1080/10168664.2020.1749012.
URL https://doi.org/10.1080/10168664.2020.1749012

[66] F. Magalhães, Álvaro Cunha, Explaining operational modal analysis with data from an arch bridge, Mechan-

ical Systems and Signal Processing 25 (5) (2011) 1431–1450. doi:https://doi.org/10.1016/j.ymssp.2010.08.001.

[67] F. Magalhães, Á. Cunha, E. Caetano, Dynamic monitoring of a long span arch bridge, Engineering Structures 30 (11) (2008) 3034–3044. doi:10.1016/j.engstruct.2008.04.020.
URL `http://dx.doi.org/10.1016/j.engstruct.2008.04.020`

[68] F. gu, H. Zhang, S. Wang, An expectation-maximization algorithm for blind separation of noisy mixtures using gaussian mixture model, Circuits, Systems, and Signal Processing 36 (2017) 2697–2726. doi:10.1007/s00034-016-0424-2.

[69] T. Hastie, R. Tibshirani, J. Friedman, The Elements of Statistical Learning Data. Data Mining, Inference, and Prediction, Springer, 2001. doi:https://doi.org/10.1007/978-0-387-21606-5.

[70] M. Sanayei, B. Arya, E. M. Santini, S. Wadia-Fascetti, Significance of Modeling Error in Structural Parameter Estimation, Computer-Aided Civil and Infrastructure Engineering 16 (1) (2004) 12–27. doi:10.1111/0885-9507.00210.

[71] L. Wang, H. Liu, Z. Chen, F. Zhang, L. Guo, Combined digital twin and hierarchical deep learning approach for intelligent damage identification in cable dome structure, Engineering Structures 274 (2023) 115172. doi:https://doi.org/10.1016/j.engstruct.2022.115172.

[72] P. Seventekidis, D. Giagopoulos, Model error effects in supervised damage identification of structures with numerically trained classifiers, Mechanical Systems and Signal Processing 184 (2023) 109741. doi:https://doi.org/10.1016/j.ymssp.2022.109741.

[73] K. H. Padil, N. Bakhary, M. Abdulkareem, J. Li, H. Hao, Non-probabilistic method to consider uncertainties in frequency response function for vibration-based damage detection using artificial neural network, Journal of Sound and Vibration 467 (2020) 115069. doi:https://doi.org/10.1016/j.jsv.2019.115069.

[74] X. Yin, Z. Huang, Y. Liu, Bridge damage identification under the moving vehicle loads based on the method of physics-guided deep neural networks, Mechanical Systems and Signal Processing 190 (January) (2023) 110123. doi:10.1016/j.ymssp.2023.110123.
URL `https://doi.org/10.1016/j.ymssp.2023.110123`

[75] J. Kullaa, Damage detection of the Z24 bridge using control charts, Mechanical Systems and Signal Processing 17 (1) (2003) 163–170. doi:10.1006/mssp.2002.1555.
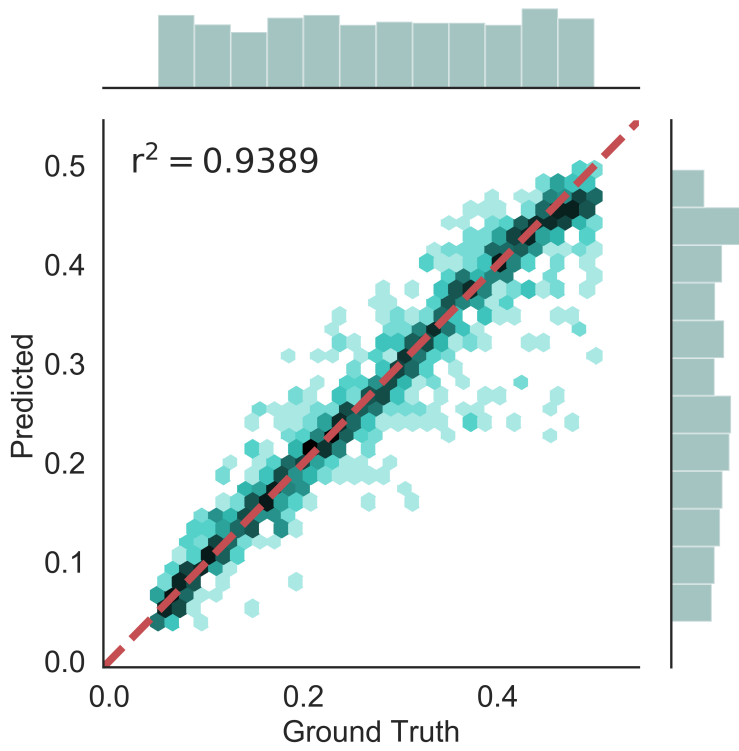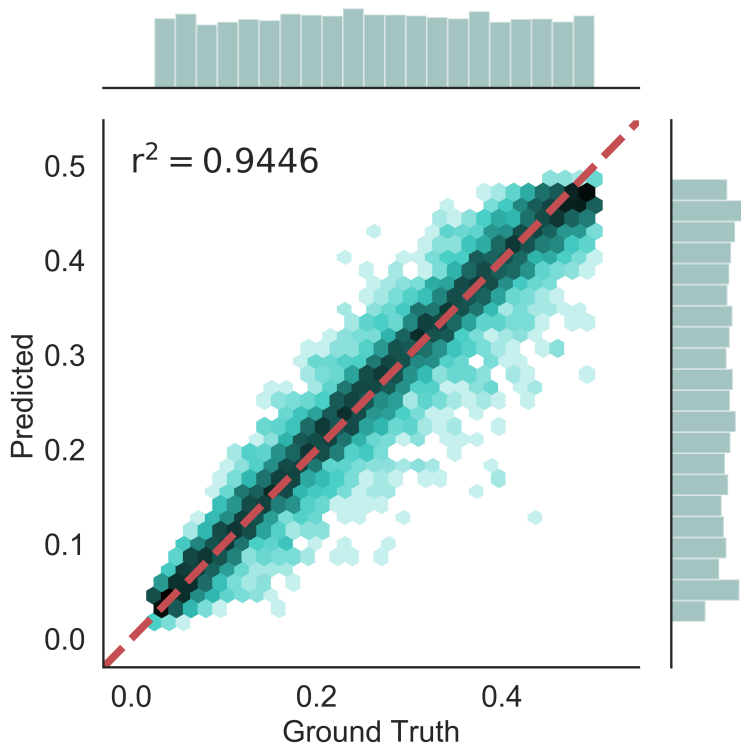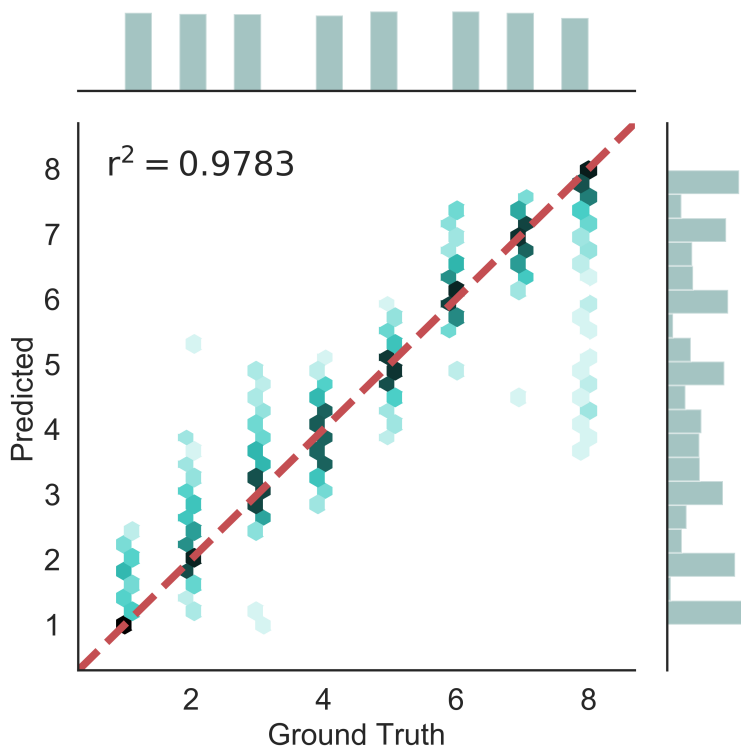
(a) Severity cross-plot under seen EOCs
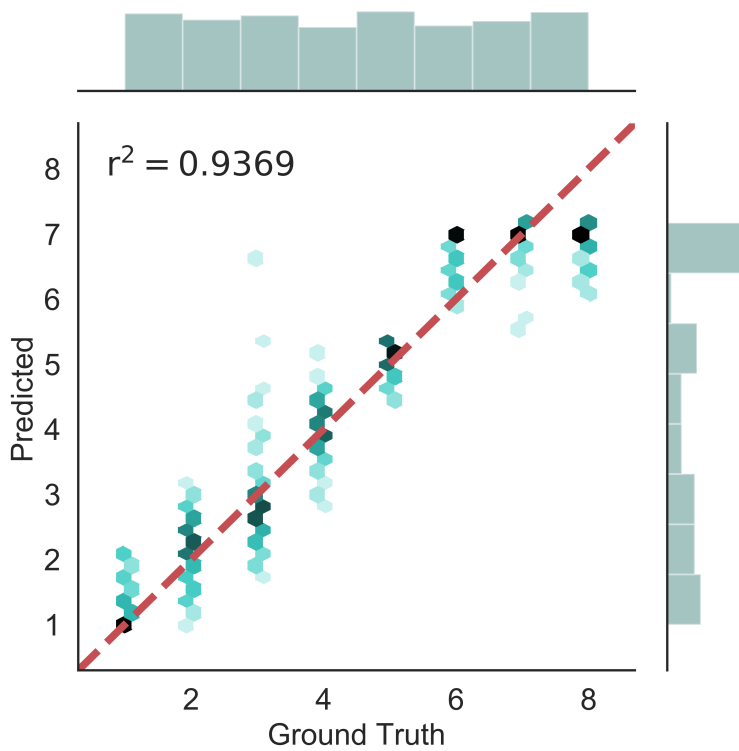
(b) Location cross-plot under seen EOCs

Figure 10: Testing cross-plots for the original approach under seen EOCs

(a) Severity cross-plot under seen EOCs.

(b) Location cross-plot under seen EOCs.

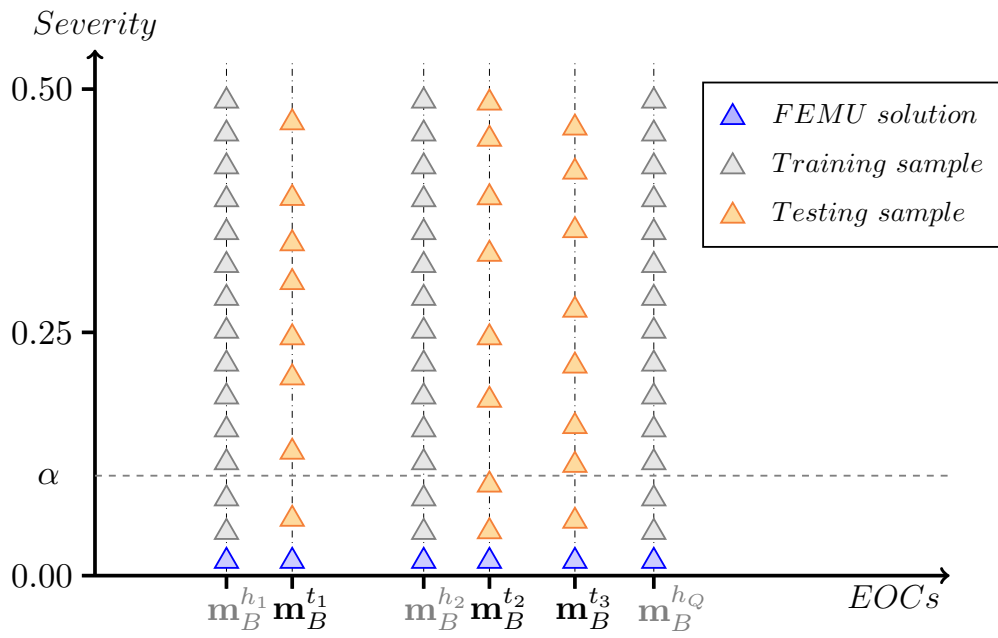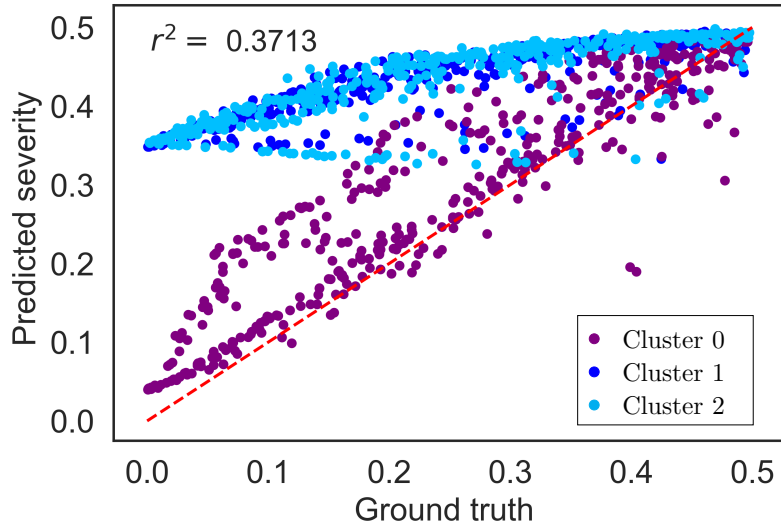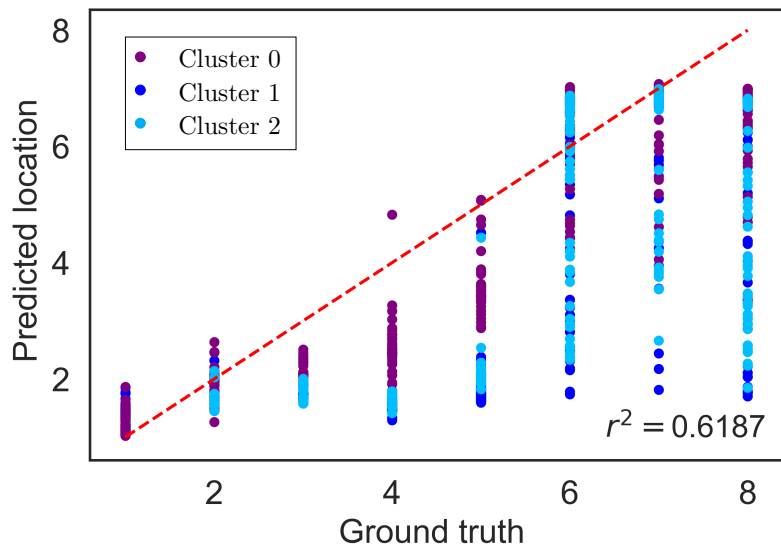Figure 11: Cross-plots during testing under seen EOCs for the new database

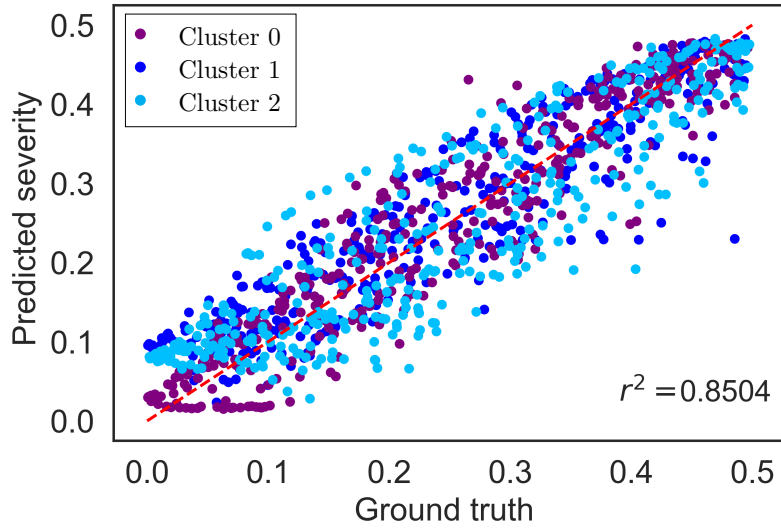Figure 12: Example of synthetic testing samples under unseen EOCs

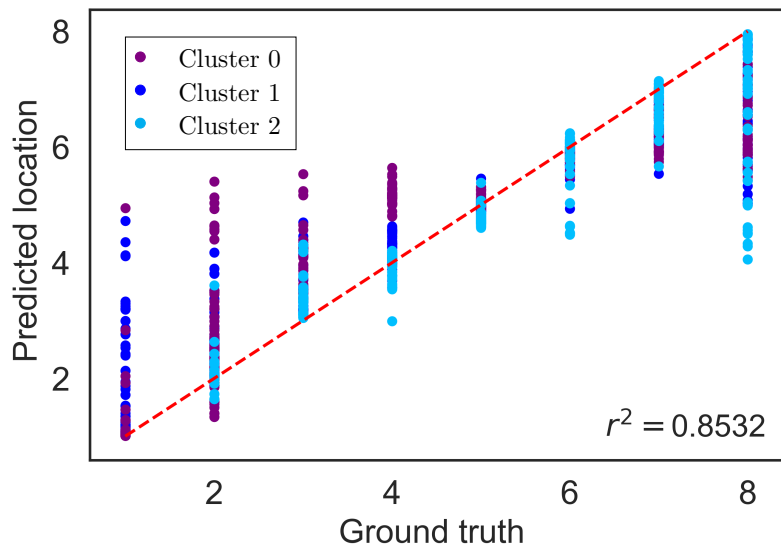(a) Severity cross-plot under unseen EOCs

(b) Location cross-plot under unseen EOCs

Figure 13: Testing cross-plots for the original database under unseen EOCs

(a) Severity cross-plot under unseen EOCs

(b) Location cross-plot under unseen EOCs

Figure 14: Testing cross-plots for the proposed approach under unseen EOCs